

RESEARCH

Open Access



Lateral Load Distribution for Hollow Slab Bridge: Field Test Investigation

Yu Zhao, Xiaozhe Cao, Yongjun Zhou*, Gangqiang Wang and Ruixin Tian

Abstract

Distribution factors (DFs) for one typical cross-section as specified in the AASHTO LRFD specification can be varied when the bridge parameters such as span length, loading lanes and skew are changed. The diversity between design and actual DFs may be varied as the bridge parameters changed. To study this diversity, this paper presents an evaluation of lateral load DFs for prefabricated hollow slab bridges. The response of the bridge was recorded during the field test. This field test was divided into two stages: a concentrated force loading test on the prefabricated girder that settled on the bridge supports before the girders were connected transversely and a vehicle loading test after the girders were connected transversely. The instruments used to record the response of the bridge were strain gauges and dial indicators. The measured data in the multi-stages of the field test could be used to calibrate the support condition of the bridge and transverse connection between adjacent girders in the finite element model (FEM) using beam and plate elements. From the FEM, DFs for this hollow slab bridge were determined and compared with the DFs in the AASHTO LRFD specification. A parametric study using the calibrated FEM was then used to investigate the effect of various parameters including span length, skew and bridge deck thickness on the DFs. It was found that AASHTO LRFD specification is conservative compared with the analysis in the FEM, while this conservatism decreased as the span length and skew of the hollow slab bridge increased.

Keywords: hollow slab bridge, field test in multi-stage, distribution factor, support condition, transverse connection

1 Introduction

Many hollow slab bridges are designed to be skewed bridges to satisfy the traffic requirements. The live-load response of this kind of bridge could be affected by span length, bridge deck thickness and skewed angle, etc. To describe and simplify the effect of these parameters, the distribution factor (DF) is proposed by assigning fractions of transmitted load amongst the primary structural members (Harris 2010; Song et al. 2003).

Most hollow slab bridges in the design plan were designed as simply supported. However, it was reported that even slight changes in boundary conditions have a considerable effect on the results (Schulz et al. 1995). Bridge test in Ontario had shown that slab-on-girder

bridges are usually significantly stiffer in flexure because of horizontal restraint provided by the girder bearings (Bakht and Jaeger 1988). Emon and Nowak (2001) proposed that the hinge-roller supports can be partially fixed (frozen) due to many factors and they found that the code-specified DF values without considering the effect of possible support fixity can be too conservative. The actual boundary condition for the bridge was quite important for analyzing the bridge structural behavior. Many field tests were conducted on the existing bridges and the field test responses were suggested to calibrate the FEM for further research (Seo et al. 2017; Hodson et al. 2011, Bechtel et al. 2010). Bridge response under loading test was the interaction of various parameters. However, field test data on the existing bridge couldn't calibrate all of these parameters. As a result, parameters had few effect on the bridge behavior were considered to be the design value in the FEM. For hollow slab bridges, adjacent girders were connected transversely by the hinge

*Correspondence: zyj@chd.edu.cn
School of Highway, Chang'an University, Xi'an 710064, People's Republic of China
Journal information: ISSN 1976-0485 / eISSN 2234-1315

joint to attract load together. For accurate analysis, transverse connection between adjacent girders and support condition are two important parameters that need to be calibrated in the FEM for this type of bridge. Multi-stage loading tests on the constructing bridge were an effective way to calibrate these two parameters, respectively.

Many studies investigated the effect of secondary elements such as parapets, sidewalk and diaphragm on the DFs and concluded that AASHTO LRFD specification was conservative without considering these secondary elements (Mabsout et al. 1997; Conner and Huo 2006; Namy et al. 2015). Geometric dimensions of the bridge remained unchanged in these studies. However, geometric dimensions of the bridge were the variables of the DF calculation formula in AASHTO LRFD specification. For a certain kind of bridge, geometric dimensions could be varied in an appropriate range. As a result, the designed DFs for different geometric dimensions were also changed in a certain range. So the effect of geometric dimensions, which were varied in a rational range, on the DFs should be figured out first before discussing the effect of secondary elements.

The aim of this study is to identify the supporting condition and transverse connection of the hollow slab bridge in the field tests using multi-stage construction of full-scale test in situ. First, a concentrated loading test was conducted on the prefabricated girder that settled on the supports before the girders were connected transversely. The response of the prefabricated girder could be used to calibrate the support condition of the hollow slab in the FEM. Second, a vehicle loading test was performed on the bridge after the prefabricated girders were transversely connected. Transverse connection between adjacent girders could be calibrated with the

bridge response under the vehicle loading test. In addition, a parametric study was conducted to investigate the influence of various parameters on the DFs of this hollow slab bridge including span length, skew and bridge deck thickness. Finally, the effect of these parameters on the DFs was quantified compared with the AASHTO LRFD specification.

2 Bridge Description

A constructing hollow slab bridge, which is located on WeiXu expressway in Henan province, China, was selected for this study. The superstructure was simply supported prefabricated concrete hollow slab girders, which was shown in Fig. 1. The span of bridge was 13 m in length with a 12.412 m clear span. The width of the bridge was 13.5 m and skewed at 25°. The hollow slab girders had a height of 0.7 m and a width of 0.99 m, and covered 0.1 m thick layer of cast-in-place reinforced deck. The bridge girders were prefabricated and the deck was cast. The connection of structures in the bridge superstructure is shown in Fig. 2. The concrete of hinge joints and bridge deck was cast at the same time. The concrete used in the slab girders, hinge joints and bridge deck had a designed compressive strength of 50 MPa and modulus of elasticity of 3.45×10^4 MPa. The superstructure was composed of 13 girders, in which the leftmost girder was denominated G1 while the rightmost girder denominated G13.

2.1 Concentrated Force Loading Test

2.1.1 General

This loading phase was performed after the prefabricated girders were installed and the adjacent girders had not been connected transversely. Before this loading test,

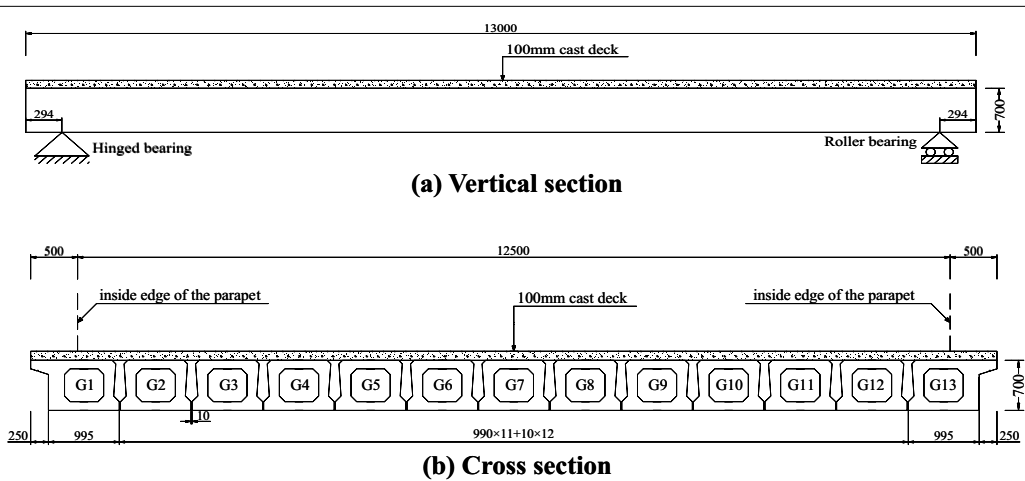


Fig. 1 Field tested bridge (units: mm).

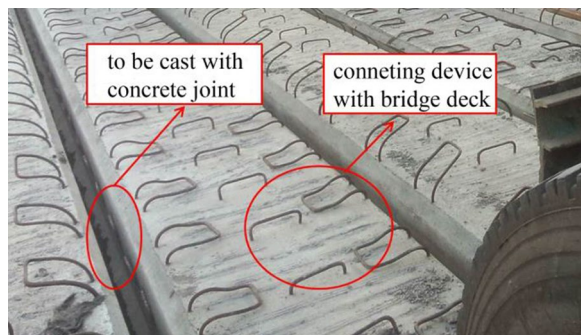


Fig. 2 Connection configuration of the bridge superstructure.



Fig. 3 Concentrated force loading test.

a preloading test was carried out on the tested girders to ensure the accuracy of the instruments. G1 (exterior girder), G4 (interior girder) and G7 (medium girder) girders were selected to be the test girders. The loading girder, which weighed 160.44 kN, was also a prefabricated hollow slab girder. One end of the loading girder was simply supported on the bearings in the mid-span of the two tested girders and the other end of the loading girder was simply supported outside the abutment (Fig. 3). As a result, the analysis of the tested girder could be simplified to be a prefabricated girder with a concentrated force on the mid-span. So the concentrated force applied on the mid-span of each tested girder was 80.22 kN. The concentrated force loading tests were performed on the G1 and G4, G4 and G7, respectively. The dimension of the girder and material properties were measured in this loading phrase.

2.1.2 Instrument Arrangement

During the loading test, four strain gauges were placed on the middle section of each tested girders to measure strains, while one dial indicator was placed to measure the mid-span deflection. Where, two dial indicators were

installed on the tested girders near the supports to measure the support settlement. The deflection caused by the concentrated force on the mid-span of the tested girder could be eventually determined. Figures 4 and 5 show the gauge configurations. Totally, for the three slabs, the gauges for the strain (D1–D12) were located on the top and bottom flanges of the girder, while the dial gauges for the mid-span deflection (DN1–DN3) were located on the bottom flange of the girder. The strain gauges were sealed by insulating tape as moisture-proof measurement. The lead wires from these gauges went through the hinge joint from the top to the bottom, so that the gauges could be used in the next loading phase after the bridge deck was cast. A strain gauge was placed on a stress free concrete as the common temperature measurement. The test data acquired in this loading phase was expected to study the actual support conditions of the tested bridge.

3 Vehicle Loading Test

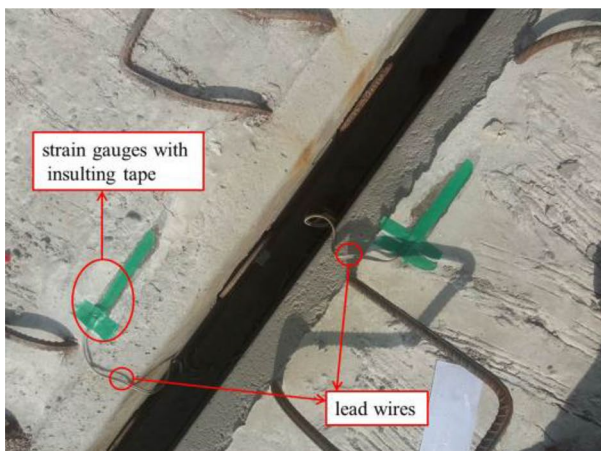
3.1 General

This loading phase was performed after the slabs were connected transversely, the bridge deck was cast and the concrete strength met the design requirements. In order to excite the normal response of the bridge, Heavy truck loaded 360 kN was used as the loading vehicle. The truck was weighed and measured before its arrival on site. Figure 6 shows the parameters of the loading vehicle.

During the loading test, the loading truck was positioned at each of the five transverse loading cases (LC) to produce different response (Fig. 7). When the loading truck was driven to the predetermined position and the engine was stalled, there was an interval of 5 min to collect the strain and deflection data until the effect of the moving truck on the bridge disappeared. Once the collection of the data was complete in one location, the loading truck was driven off the bridge and waited for 5 min so that the deformation of the tested girder could be restored, then, the vehicle loading test could be performed again on the next transverse location. Loading and unloading tests were performed repeatedly to acquire test data.

3.2 Instrument Arrangement

Strain gauges and dial indicators were all installed on the bottom of the mid-span section of the girder (Fig. 8). In which, six gauges that were mounted in the top flange of the three girders in the former loading test were also used in this loading phase to measure the strain of the top flange. Again, two indicators were placed at the supports and one indicator was placed in the mid-section for each girder. Consequently, there were 19 strain gauges and 39 dial indicators in this loading phase.



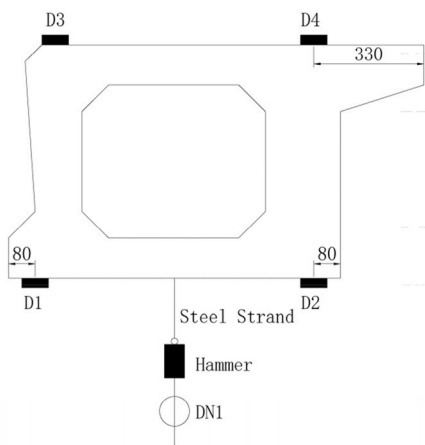
(a) Strain gauges on the top flange of the girder



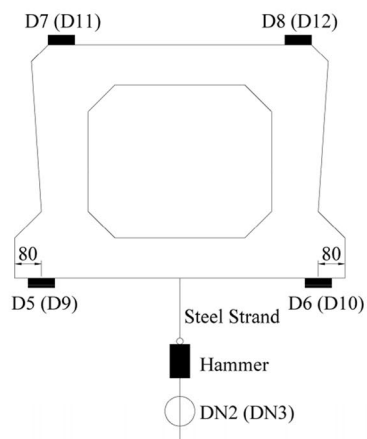
(b) Strain gauges on the bottom flange of the girder



(c) Dial indicator

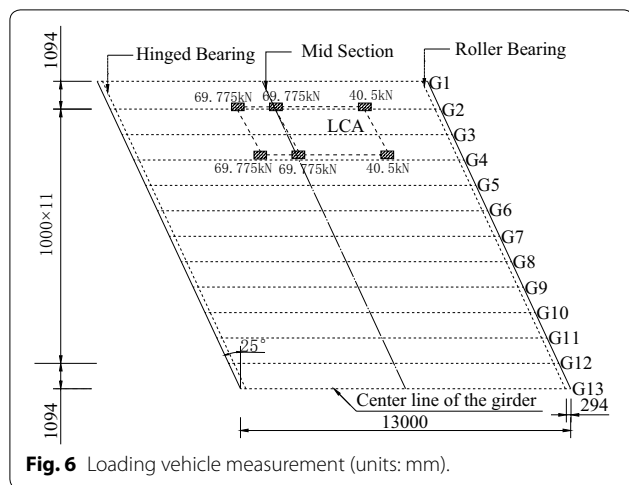
Fig. 4 Strain and deflection gauges.

(a) Measurement instrument on the mid section of the G1 girder



(b) Measurement instrument on the mid section of the G4 (G7) girder

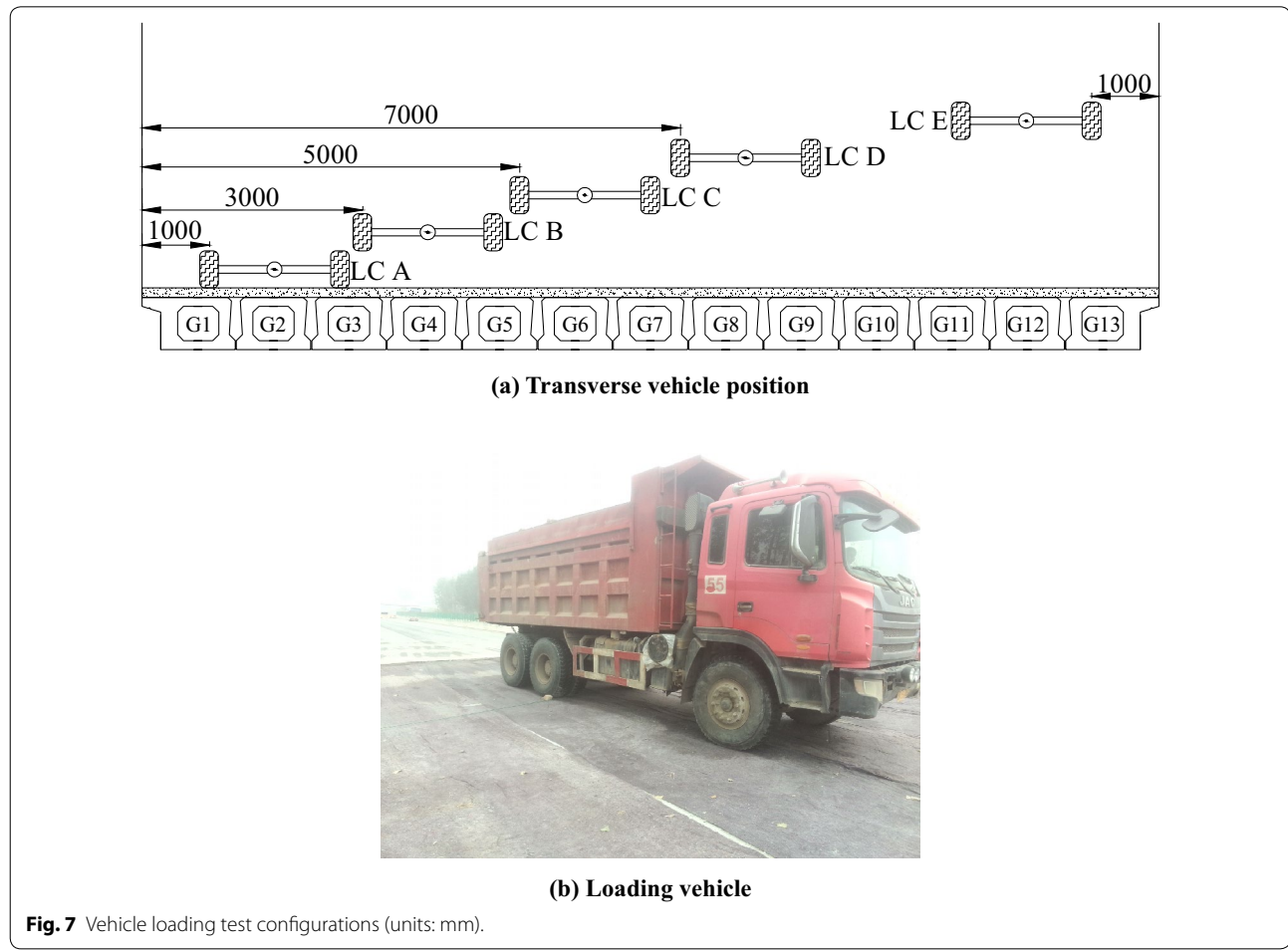
Fig. 5 Measurement instrument position (units: mm). Note: Di: strain gauges; DNi: deflection gauges.

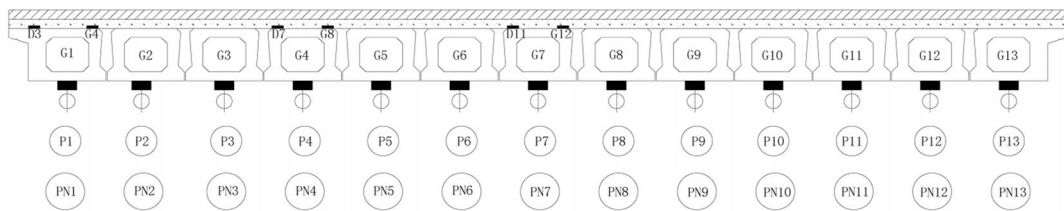


4 Finite-Element Model

In order to assure the correction of the finite element analysis (FEA), two different FEA programs—MIDAS CIVIL and ANSYS were conducted. In MIDAS CIVIL,

the main girder and virtual transverse beam were modeled by the beam element while the bridge deck was modeled by the plate elements. In ANSYS program, beam188 elements were used to model the main girder and virtual transverse beam, shell63 element were used to model bridge deck. For the beam element in MIDAS CIVIL and ANSYS, each node for these elements had three translational degrees of freedom and three rotational degrees of freedom. As for the plate element and shell63 element, there were six degrees of freedom at each node were used to model bridge deck. Material and structural properties in the FEM were based on the bridge design plan as well as the collected and measured information about the bridge supplemented with engineering judgment(Seo et al. 2015). The concrete grade using for the girder, hinge joint and bridge deck is C50, The modulus of elasticity of the concrete is 3.45×10^4 MPa. As specified in the AASHTO LRFD specification, live load deflection is a service issue, not a strength issue. So in the calculation of the FEM, the nonlinearity of the concrete materials was not considered. Figure 9 shows the FE models of the bridge.





(a) Instrument position in mid-span of the girders



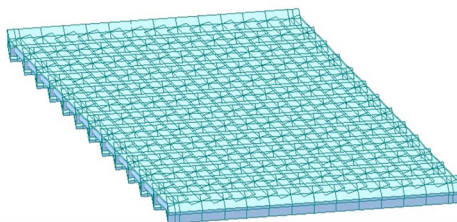
(b) Instrument position in bearings



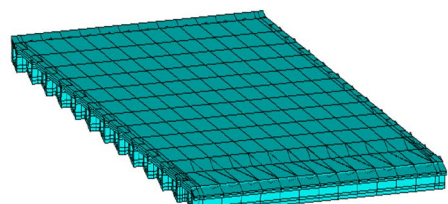
(c) deflection gauges



(d) Deflection gauges

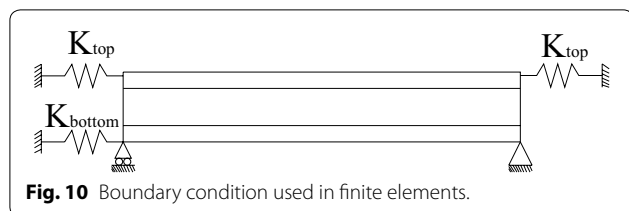
Fig. 8 Instrument arrangement in the vehicle loading test. Note: Pi: strain point, PNi: deflection point.

(a) MIDAS CIVIL model



(b) ANSYS model

Fig. 9 Finite element models.



4.1 Boundary Conditions

Elastic spring elements were used to simulate actual behavior of supports as shown in Fig. 10 (Eom and Nowak 2001). To model this kind of connection, general connection options in elastic connection were selected in MIDAS CIVIL, while the combin14 elements were modeled in ANSYS model. In this calibrating process, main girders were not connected transversely. Elastic spring elements were added to restrict the horizontal movement of the bridge on the base of the simply support condition according to the design plan. The stiffness of the spring elements was represented by K values. The suitable K values were found by comparing the deflections at the mid-span from FEM analysis with those from the concentrated force loading test by trial and error analysis. The K values used in the analysis are shown in Table 1, in which, girder 1 and 13 had different K values with the other girders because of their different section from the others. The K values that acquired from different FE models were the same.

4.2 Transverse Connection

After the boundary conditions of the FEM were determined, transverse connections between adjacent girders were calibrated with the field test data acquired in vehicle loading tests. 100 mm thick plate elements and shell63 elements were included in this modeling phrase

to simulate the effect of bridge deck. Beam elements and beam188 elements used for transverse connection between adjacent girders were defined as virtual transverse beam elements, which had no quality but only transverse stiffness between adjacent girders. The cross sections of virtual transverse beams were rectangles with a width of 1000 mm. The height of the virtual transverse beam was iterated to fit the test results. The truck loads were applied as concentrated loads and were positioned on the FEM as presented in the vehicle loading test. By trial and error, the suitable virtual transverse beam height was determined by comparing correlation and error between FEM and field test responses. Percent error, δ_p , and correlation coefficient, ρ (Seo et al. 2017) were used in the comparison:

$$\delta_p = 100 \cdot \left[\frac{\sum (\omega_f - \bar{\omega}_f)^2}{\sum (\omega_f)^2} \right] \quad (1)$$

$$\rho = \left[\frac{\sum (\omega_f - \bar{\omega}_f)(\omega_a - \bar{\omega}_a)}{\sum \sqrt{(\omega_f - \bar{\omega}_f)^2(\omega_a - \bar{\omega}_a)^2}} \right] \quad (2)$$

where ω_f , ω_a , $\bar{\omega}_f$ and $\bar{\omega}_a$ = field deflection response, FEM deflection responses, sample mean values of ω_f , and sample mean values of ω_a , respectively.

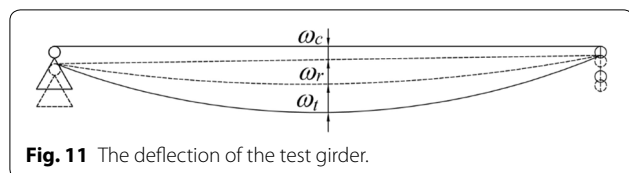
Virtual transverse beam height with highest correlation coefficient and the lowest percent error was determined to be the ultimate height. Table 2 presents a summary of the percent errors and correlation coefficients among different virtual transverse beam heights. The correlation coefficients of different transverse beam heights are 1, which means using virtual transverse beam method could simulate transverse connection of adjacent girders pretty well. Virtual transverse beam with 300 mm height

Table 1 Spring coefficients used in FEM.

FEA program	Girder number	1#	2#	3#	4#	5#	6#	7#	8#	9#	10#	11#	12#	13#
MIDAS CIVIL/ANSYS	K_{top} (kN/mm)	630	770	770	770	770	770	770	770	770	770	770	770	630
	K_{bottom} (kN/mm)	630	770	770	770	770	770	770	770	770	770	770	770	630

Table 2 Model accuracy for different virtual transverse beam heights.

	Virtual transverse beam height (mm)	100	200	300	400	500	600	700
MIDAS CIVIL	δ_p (%)	12.97	5.88	5.32	6.46	8.06	9.75	11.37
	ρ	1	1	1	1	1	1	1
ANSYS	δ_p (%)	9.32	8.84	6.91	9.17	10.03	10.55	11.36
	ρ	1	1	1	1	1	1	1



has the lowest percent error in both FEM analyses. So the virtual transverse beam with a width of 1000 mm and a height of 300 mm was found to forecast most closely actual transverse connections between adjacent girders.

5 Live Load Distribution Factors

The actual DF of each girder can be calculated using the experimental deflection data. The effective deflection under vehicle loading was calculated by the following Eq. 3 as shown in Fig. 11.

$$\omega_e = \omega_t - \omega_r - \omega_c \quad (3)$$

where ω_e is the effective measured deflection of girders under loads, ω_t is the total measured deflection of girders, ω_r is the measured residual deflection of girders, ω_c is the measured deflection at both ends of girders.

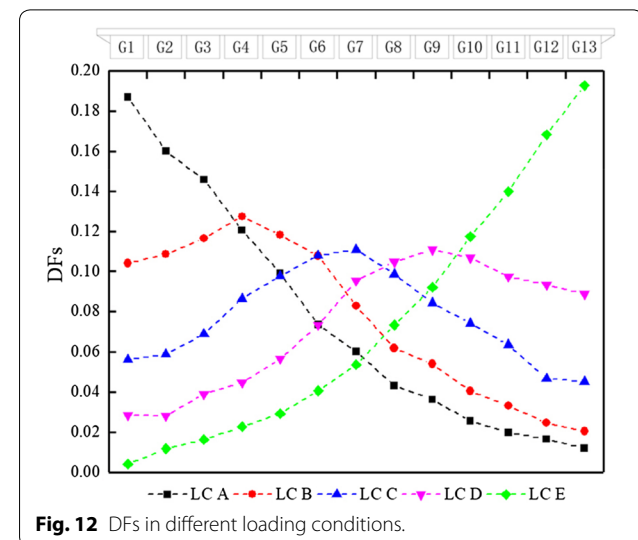
The formula used here to calculate DF for the i th girder is Eq. 4 (Harris et al. 2008), which has been widely used in many live-load tests (Civitillo et al. 2014; Harris et al. 2016; Waldron et al. 2005). These DFs are representative of a single-truck loading resisted by each girder. DFs in five different loading conditions were shown in Fig. 12.

$$DF_i = \left(\frac{\omega_i}{\sum_{i=1}^{13} \omega_i} \right) \times N_{\text{vehicles}} \quad (4)$$

where, DF_i is load distribution factor of i th girder; ω_i is maximum deflection of i th girder; N_{vehicles} is the number of vehicles on the bridge.

It can be concluded that the girder which suffered the traffic load directly experiences the greatest deflection, whereas girders far away from the loading position experience less. DFs for exterior girder were 52% greater than the DFs for the most heavily loaded interior girder, the reason is that in this test there are no railings which usually offered a significant stiffening contribution to the exterior girders and the exterior girder is unable to distribute load to an interior member.

Figure 13 shows the deflections at mid-span on each girder under different loading conditions. It can be seen from Fig. 13 that the deflection curves were nearly overlapped for the five loading conditions. It can be



concluded that the FEM is reliable to conduct further researches.

Distribution factors for single and multilane loaded are different in AASHTO specification. Only one lane loaded was conducted in the field test. The number of lane was changed in the calibrated FEM to observe the deflection of girders. The loading vehicle used in the FEM was the same as it used in field test and the vehicle wheel loads were applied as concentrated loads in the FEM. The bridge was divided into three 3.75 m-wide-lanes. FEM with concentrated load was shown in Fig. 14. Loading vehicles were positioned on the middle of each lane laterally. The longitudinal position of trucks was calculated as the position producing the maximum bending moment at midspan. The number and position of the load vehicles were systematically varied to consider all possible load combinations. In all cases the vehicles were placed following the 25° skew.

Interior and exterior distribution factors are calculated separately in the AASHTO specification. As such, the maximum distribution factor for the one, two and three loaded lanes for both the interior and exterior girders were calculated using the maximum deflection of different girders. Calculated moment DFs for the interior and exterior girders for each load cases are listed in Table 3. DFs calculated by the AASHTO LRFD were also listed in Table 3.

Table 3 shows that using AASHTO LRFD specifications resulted in a conservative DFs estimate. The AASHTO DFs were much higher than those calculated using the calibrated FEM for exterior girders. For one lane loaded, the AASHTO LRFD DFs were 1.5 times larger than that of the FEM DFs for exterior girders and 1.2 times larger for interior girders. For multilane loaded, the AASHTO

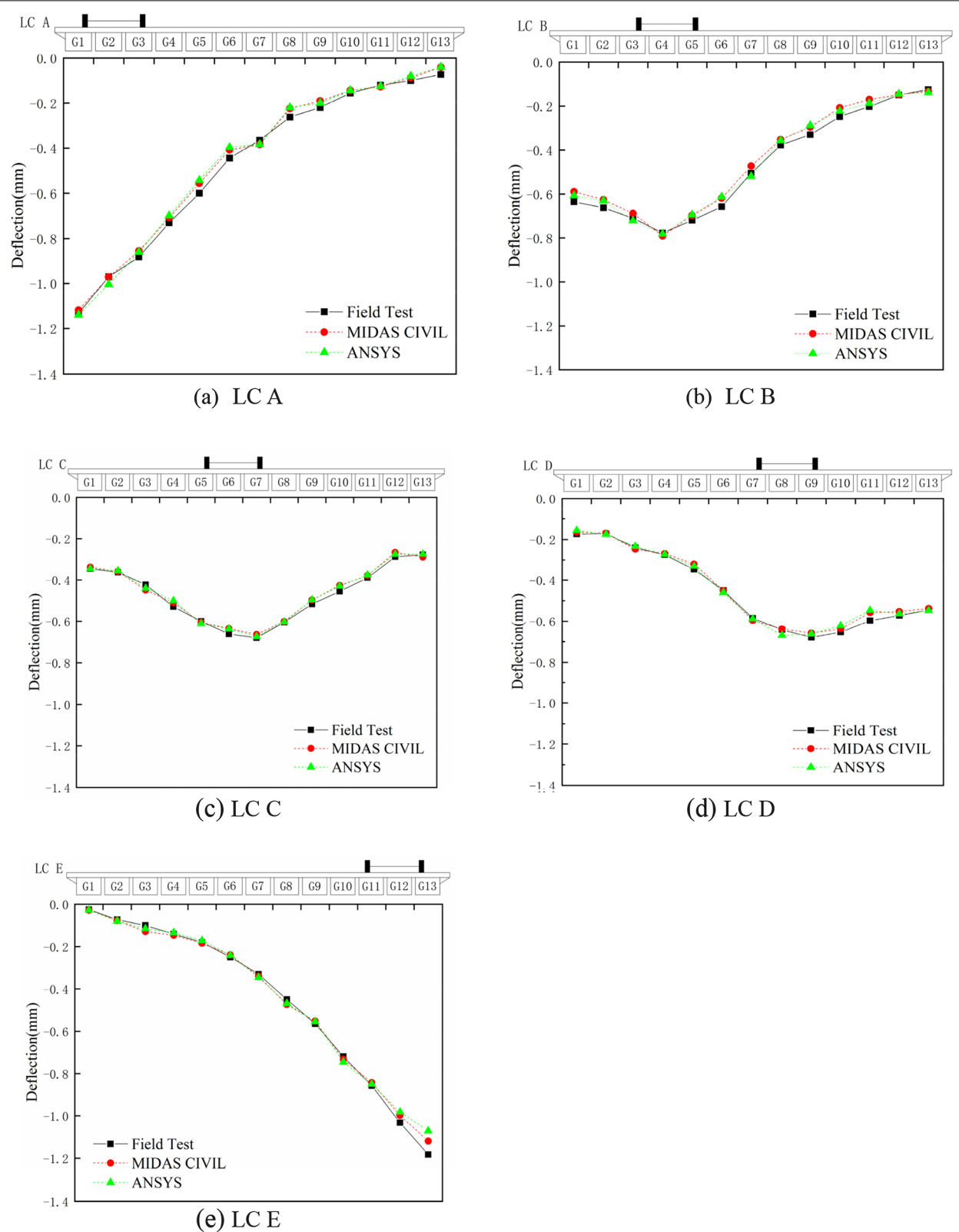


Fig. 13 Deflection distribution in different loading conditions.

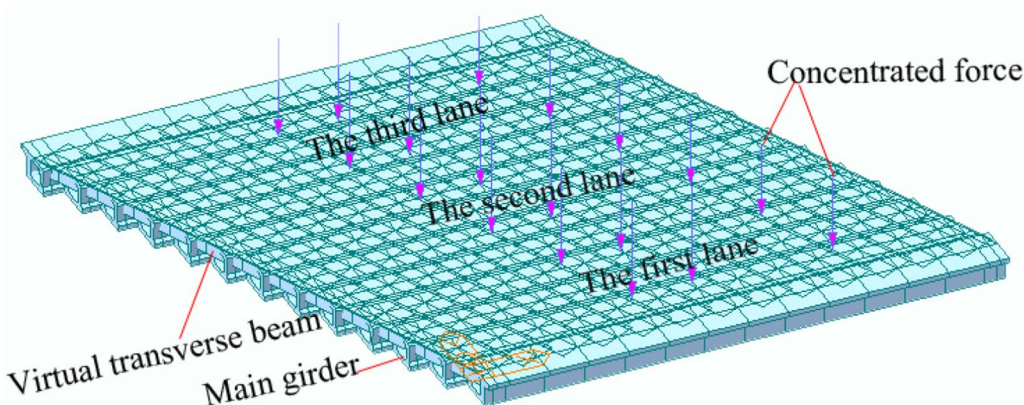


Fig. 14 FEM with three loaded lanes.

LRFD DFs were 1.4 times larger than that of the FEM DFs for exterior girders and were very close to the FEM DFs for interior girders. DFs for exterior girder were controlling DFs in AASHTO LRFD specification, while the controlling DFs were interior girder DFs in the FEM. This is probably caused by the lack of parapets in the FEM, which could provide stiffness for the exterior girders. DFs for interior girder in AASHTO LRFD specification was 1% to 18% higher than the DFs in FEM. For exterior girder, DFs of AASHTO LRFD specification was 37% to 48% higher than the DFs in FEM.

As the loading lane increased from one to two in the FEM, DFs increased 17% for exterior girders and 34% for interior girder. While as the loading lane increased from two to three, the DFs increased by 2% and 9% for exterior and interior girders, respectively. DFs could be different for one lane loaded and two lanes loaded, but less difference for two lanes loaded and three lanes loaded. In multilane loaded cases, DFs of three loaded lanes were more closed to the AASHTO LRFD specification compared with the DFs of two loaded lanes. When the bridge

was filled with vehicles on the lanes that it can be divided into, the DFs were more closed to the AASHTO LRFD specification for this multilane loaded case.

6 Parametric Study

A parametric study was performed for hollow slab bridge to investigate the parameters affecting the DFs of vehicle loads. The effect of parameters on the DFs were quantified and compared with AASHTO LRFD specifications. Span length, bridge skew and bridge deck thickness were three major parameters in this parametric study. A baseline FEM was determined using the dimensions and supporting conditions of the field tested bridge. The baseline model was adjusted to study the effect of one parameter while the other parameters were kept in the baseline value. While changes in certain parameters (i.e., span length) do affect other parameters (i.e., girder stiffness), the effect was minimal and they could be evaluated independently (Zokaie 2000). Therefore, span length was varied from 8 to 20 m, which was the specified length of the hollow slab bridge, in the FEM. The effect of skew was investigated by adjusting the skew angle from 0 to 60°. The bridge deck thickness was varied from 0.1 m to 0.5 m by adjusting the thickness of plate element. DFs calculated from the FEM were compared with those calculated ones according to the AASHTO LRFD specifications, this ratio of which could reflect the difference between FEM and AASHTO LRFD specifications.

DFs for one loaded lane and three loaded lanes were calculated in the Table 4 to investigate the effect of span length. It can be seen from Table 4 that DFs for exterior girder increased 10% for one loaded lane and 42% for three loaded lanes, while for interior girder, DFs decreased 30% for one loaded lane and 9% for three loaded lanes. As the DFs calculated by MIDAS CIVIL and ANSYS were really close, so the DFs in Fig. 15 were

Table 3 Distribution factors for different number of lanes.

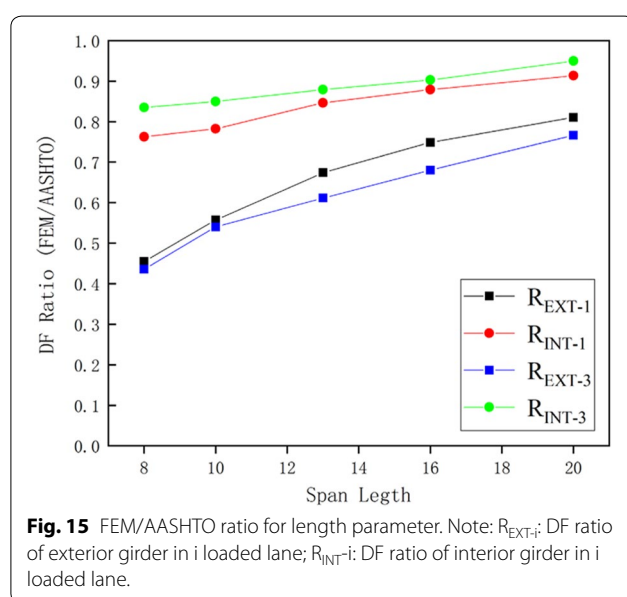
Number of lanes	Calculation method	DF _{EXT}	DF _{INT}
One lane	AASHTO LRFD	0.230	0.202
	MIDAS	0.155	0.171
	ANSYS	0.155	0.175
Two lanes	AASHTO LRFD	0.265	0.255
	MIDAS	0.183	0.231
	ANSYS	0.180	0.233
Three lanes	AASHTO LRFD	0.265	0.255
	MIDAS	0.193	0.252
	ANSYS	0.190	0.252

DF_{EXT} distribution factor of exterior girder; DF_{INT} distribution factor of interior girder.

Table 4 DFs for span parameter in the FEM.

Span (m)	8		10		13		16		20	
	MIDAS	ANSYS								
DF _{EXT-1}	0.136	0.132	0.147	0.147	0.155	0.155	0.155	0.155	0.150	0.147
DF _{INT-1}	0.205	0.209	0.177	0.174	0.171	0.175	0.160	0.163	0.148	0.145
DF _{EXT-3}	0.148	0.145	0.175	0.171	0.193	0.190	0.200	0.197	0.210	0.206
DF _{INT-3}	0.269	0.272	0.261	0.263	0.252	0.255	0.251	0.251	0.246	0.249

DF_{EXT-i} distribution factor of exterior girder for i loaded lane; DF_{INT-i} distribution factor of interior girder for i loaded lane.



the average values of the DFs in two different FEM analyses. In Fig. 15, DF ratios increased and were closed to 1 as the span length increased for both one loaded lane and three loaded lanes. This trend showed that AASHTO LRFD specification became less conservative as the span length increased. The ratio of the FEM to AASHTO distribution factor for exterior girder ranged from 0.45 to 0.81 for one loaded lane and from 0.45 to 0.76 for three loaded lanes. While for interior girder, the ratio of the FEM to AASHTO LRFD specification distribution factor was 0.76 to 0.91 for one lane and 0.84 to 0.95 for three

lanes. The lack of parapets in the FEM, which could provide stiffness for the exterior girder, made the DF of exterior girder lower than that of interior girder.

DFs in different bridge skew were shown in Table 5. Compared with the DFs of the straight bridge (of which the skew is 0°), the DFs decreased 5% for exterior girder and 4% for interior girder when the bridge skew was 5° . For exterior girder, DFs were not changed for the skew of 10° , 15° and 25° , while the DFs decreased 3% to 11% as the skew increased from 35° to 60° . DFs of interior girder were not changed as the skew increased from 10° to 45° and the DFs increased 3% when the skew was 60° . DFs in Fig. 16 were also the average DF values of two different FEM analyses. It can be seen in the Fig. 16 that AASHTO became less conservative as the skew increased from 10° . The ratio of FEM and AASHTO was greater than 1 for interior girder when the skew was 60° , while the DFs of exterior girder were less than design value for each of skew angle.

The calculation results from MIDA CIVIL and ANSYS were pretty close. DFs in Fig. 17 were the average values of the two FEM analyses. DFs for exterior girder increased 4% and 5% for one and three loaded lanes, respectively, while for interior girder, DFs decreased 3% and 2% for one and three loaded lanes, respectively. Neither the DF of exterior nor the interior girder was influenced by the deck thickness significantly in Fig. 17.

7 Conclusions

A hollow slab bridge was subjected to a live-load test and detailed FE analyses. DFs for AASHTO LRFD specification and actual bridge were compared. In addition,

Table 5 DFs for skew parameter in the FEM.

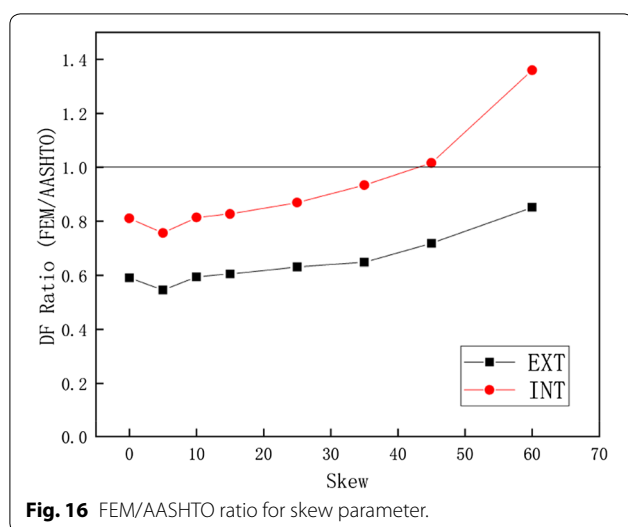


Fig. 16 FEM/AASHTO ratio for skew parameter.

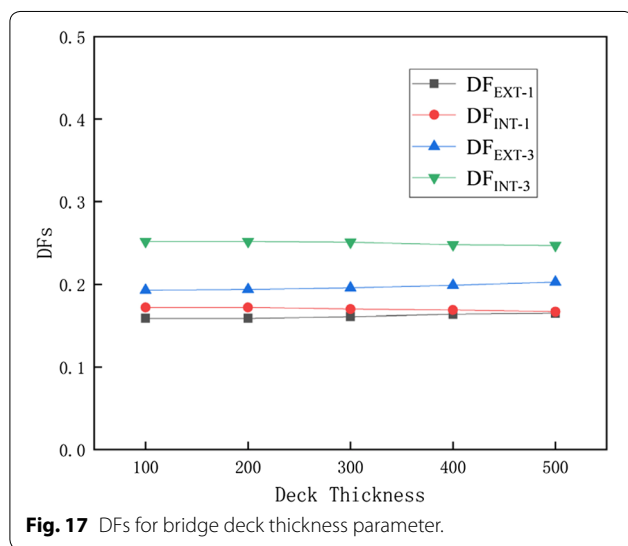


Fig. 17 DFs for bridge deck thickness parameter.

the effects of span length, skew and bridge deck thickness on the DFs were also investigated in the parametric study. From the analyses, the following conclusions were obtained:

- Compared with the DFs in the FEM of this hollow slab bridge, AASHTO LRFD DFs for interior girder (1–18%) were less conservative than exterior girder (37–48%).
- The AASHTO LRFD specification became less conservative (8%) when the loading vehicles were filled in the lane that the bridge can be divided to for multilane loaded cases.
- AASHTO LRFD specification became less conservative as the span length increased for this hollow slab

bridge. DFs of exterior girder increased 10–42% while of interior girder decreased 9–30% as the span length increased.

- AASHTO LRFD specification became less conservative as the skew was greater than 10°. DFs of FEM for interior girder were 1.4 times larger than the DFs in AASHTO LRFD specification when the skew was 60°, while the DFs of exterior girder were less than design value with an increase in the skew.
- Deck thickness had little effects on the DFs of hollow slab bridge.

8 Discussion

The parapets have been proved to provide more stiffness to the exterior girder compared with the interior girders (Barker 2001; Zhou et al. 2015). As the vehicle loading test was conducted on the bridge before the parapet was constructed, the parapets were not modeled in the FEM. So the effect of the parapets on DFs was not discussed in this paper.

Acknowledgements

The authors thank Zhongguo John Ma for his assistance during writing this paper and Wanfeng Liu and Dong Zheng for their assistance during the field tests.

Authors' contributions

YZ proposed the aim of the research and designed the field test. GW and RT conducted the field test and collected the test data. XC and YZ analyzed and interpreted the test data regarding the live load distribution. YZ was a major contribution in writing the manuscript. All authors read and approved the final manuscript.

Funding

Financial support by the key research platform open fund project of China No. 310821171121, National Science Foundation of China under Grant Nos. 51678061 and 51978063.

Availability of data and materials

The datasets used and analyzed during the current study are available from the corresponding author on reasonable request.

Competing interests

The authors declare that they have no competing interests.

Received: 6 September 2019 Accepted: 31 January 2020

Published online: 20 April 2020

References

- Bakht, B., & Jaeger, L. G. (1988). Bearing restraint in slab-on-girder bridges. *Journal of Structural Engineering*, 114, 2724–2740.
- Barker, M. G. (2001). Quantifying field-test behavior for rating steel girder bridges. *Journal of Bridge Engineering*, 6, 254–261.
- Bechtel, A., McConnell, J., & Chajes, M. (2010). Ultimate capacity destructive testing and finite-element analysis of steel I-girder bridges. *Journal of Bridge Engineering*, 16, 197–206.
- Civitillo, J. M., Harris, D. K., Gheytasi, A., Saliba, M., & Kassner, B. L. 2014. In-service performance and behavior characterization of the hybrid composite bridge system—A case study. arXiv preprint [arXiv:1409.2447](https://arxiv.org/abs/1409.2447).

- Conner, S., & Huo, X. S. (2006). Influence of parapets and aspect ratio on live-load distribution. *Journal of Bridge Engineering*, 11, 188–196.
- Eom, J., & Nowak, A. S. (2001). Live load distribution for steel girder bridges. *Journal of Bridge Engineering*, 6, 489–497.
- Harris, D. K. (2010). Assessment of flexural lateral load distribution methodologies for stringer bridges. *Engineering Structures*, 32, 3443–3451.
- Harris, D. K., Civitillo, J. M., & Ghetas, A. (2016). Performance and behavior of hybrid composite beam bridge in Virginia: Live load testing. *Journal of Bridge Engineering*, 21, 04016022.
- Harris, D. K., Cousins, T., Murray, T. M., & Sotelino, E. D. (2008). Field investigation of a sandwich plate system bridge deck. *Journal of Performance of Constructed Facilities*, 22, 305–315.
- Hodson, D. J., Barr, P. J., & Halling, M. W. (2011). Live-load analysis of post-tensioned box-girder bridges. *Journal of Bridge Engineering*, 17, 644–651.
- Mabsout, M. E., Tarhini, K. M., Frederick, G. R., & Kobrosly, M. (1997). Influence of sidewalks and railings on wheel load distribution in steel girder bridges. *Journal of Bridge Engineering*, 2, 88–96.
- Namy, M., Charron, J.-P., & Massicotte, B. (2015). Structural behavior of bridge decks with cast-in-place and precast concrete barriers: Numerical modeling. *Journal of Bridge Engineering*, 20, 04015014.
- Schulz, J. L., Commander, B., Goble, G. G., & Frangopol, D. M. (1995). Efficient field testing and load rating of short-and medium-span bridges. *Structural Engineering Review*, 3, 181–194.
- Seo, J., Kilaru, C., Phares, B. M., & Lu, P. (2015). Live load distribution factors for a short span timber bridge under heavy agricultural vehicles. *Structures Congress*, 2015, 2164–2173.
- Seo, J., Teja Kilaru, C., Phares, B., & Lu, P. (2017). Agricultural vehicle load distribution for timber bridges. *Journal of Bridge Engineering*, 22, 04017085.
- Song, S.-T., Chai, Y., & Hida, S. E. (2003). Live-load distribution factors for concrete box-girder bridges. *Journal of bridge engineering*, 8, 273–280.
- Waldron, C. J., Cousins, T. E., Nassar, A. J., & Gomez, J. P. (2005). Demonstration of use of high-performance lightweight concrete in bridge superstructure in Virginia. *Journal of performance of Constructed Facilities*, 19, 146–154.
- Zhou, Y. J., Ma, Z. J., Zhao, Y., Shi, X. W., & He, S. H. (2015). Improved definition of dynamic load allowance factor for highway bridges. *Structural Engineering and Mechanics*, 54, 561–577.
- Zokaei, T. (2000). AASHTO-LRF live load distribution specifications. *Journal of Bridge Engineering*, 5, 131–138.

Publisher's Note

Springer Nature remains neutral with regard to jurisdictional claims in published maps and institutional affiliations.

Submit your manuscript to a SpringerOpen® journal and benefit from:

- Convenient online submission
- Rigorous peer review
- Open access: articles freely available online
- High visibility within the field
- Retaining the copyright to your article

Submit your next manuscript at ► springeropen.com